Talanta 134 (2015) 435–442

Contents lists available at ScienceDirect

Talanta

journal homepage: www.elsevier.com/locate/talanta

Development and application of tetrabromobisphenol A imprinted electrochemical sensor based on graphene/carbon nanotubes three-dimensional nanocomposites modified carbon electrode

Zhaohui Zhang [a,b,*], Rong Cai [a], Fang Long [a], Jing Wang [a]

[a] College of Chemistry and Chemical Engineering, Jishou University, Hunan 416000, PR China
[b] State Key Laboratory of Chemo/Biosensing and Chemometrics, Hunan 410082, PR China

ARTICLE INFO

Article history:
Received 19 September 2014
Received in revised form
14 November 2014
Accepted 19 November 2014
Available online 26 November 2014

Keywords:
Imprinted electrochemical sensor
Tetrabromobisphenol A
Graphene and carbon nanotubes
Three-dimensional nanocomposites
Carbon electrode

ABSTRACT

A novel imprinted electrochemical sensor based on graphene/carbon nanotubes three-dimensional (3D) nanocomposites modified carbon electrode was developed for the determination of tetrabromobisphenol A. The imprinted film was prepared by one-step electrodeposition technique with pyrrole as the functional monomer and tetrabromobisphenol A as the template molecule. The imprinted sensor was used for the determination of tetrabromobisphenol A with differential pulse voltammetry. A linear relationship between the response currents and the negative logarithm of tetrabromobisphenol A concentrations was obtained in the concentrations range of 1.0×10^{-11}–1.0×10^{-8} mol L^{-1} with a detection limit of 3.7×10^{-12} mol L^{-1} (S/N=3). The proposed imprinted sensor showed excellent selectivity towards tetrabromobisphenol A. With good reproducibility and stability, the imprinted electrochemical sensor was used to detect tetrabromobisphenol A in fish samples successfully with the recoveries of 93.3–107.7%.

1. Introduction

Brominated flame retardants (BFRs), which have been used in commercial and industrial applications worldwide, have attracted tremendous attentions because of their increasing environmental toxicity [1,2]. Tetrabromobisphenol A (TBBPA), one of the commonly used BFRs, has been used in the manufacturing of office and home electronic equipment involving computer, mobile phone, television, and washing machine [3]. However, TBBPA can release into the environment from the products, which has been detected in air, soil, sediment, birds, fish, and humans [4–7]. Studies showed that TBBPA is toxic to primary hepatocytes and weak estrogen-like properties [8]. Currently, traces of TBBPA in the environment has been detected by liquid chromatography tandem mass spectrometry, high performance liquid chromatography–electro-spray tandem mass spectrometry, gas chromatography–electron capture negative-ionization mass spectrometry and luminescent sensor [9–12]. Nevertheless, time-consuming sample pretreatment and expensive instruments have limited their application. While electrochemical sensors can be considered as an alternative method for the determination of TBBPA based on their advantages of fast response, cheap instrument, simple operation, time-saving, high sensitivity, and real-time detection in situ applied to medical [13], biological [14], and environmental analysis [15]. Although our group has fabricated imprinted polymer/graphene modified electrode to detect TBBPA [16,17], there are no electrochemical sensors based on three-dimensional (3D) nanocomposites modified carbon electrode for the determination of TBBPA.

Graphene (Gr), a 2D carbon material comprised of a single sheet of hexagonally packed carbon atoms, has attracted tremendous attentions due to its unique electrical, physical and optical properties. The unique nanostructure showed great promise for potential applications in nanomaterials and nanotechnologies. However, graphene is also likely to form irreversible agglomerates via van der Waals force during the drying process [18]. Fortunately, there is interesting in introducing 1D carbon nanotubes (CNTs) with 2D Gr sheets to prevent face-to-face agglomeration, in which CNTs not only play an additional role of bridge for electron transfer between Gr sheets, but also can effectively prevent the irreversible aggregation of Gr sheets [19]. Therefore, the graphene/carbon nanotubes (Gr/CNTs) 3D nanocomposites are expected to improve the unique potential of Gr or CNTs as a free-standing electrode for electrode materials. Recently, the 3D Gr/CNTs nanocomposites have been applied in the field of supercapacitors [20,21], transparent conductors [22], and lithium ion batteries [23,24].

Molecularly imprinted polymers (MIP) are cross-linked polymers with specific recognition property for the template molecule

* Corresponding author at: College of Chemistry and Chemical Engineering, Jishou University, Hunan 416000, PR China. Tel.: +86 743 8563911/ fax: +86 743 8563911.
E-mail address: zhaohuizhang77@163.com (Z. Zhang).

http://dx.doi.org/10.1016/j.talanta.2014.11.040
0039-9140/

[25,26]. Currently, many imprinted electrochemical sensors have been developed with specific selectivity for the template [27,28]. However, there is no work reported on MIP-sensor based on Gr/CNTs 3D nanocomposites modified electrode for the determination of TBBPA.

In this work, a feasible chemical method was developed to synthesize Gr/CNTs 3D nanocomposites coated onto the bare carbon electrode firstly. Then, an imprinted film with high selectivity toward TBBPA was fabricated on the Gr/CNTs 3D nanocomposites modified carbon electrode using a one-step electrodeposition technique with pyrrole as the monomer and TBBPA as the template molecule. Scanning electron microscopy (SEM), cyclic voltammetry (CV) and differential pulse voltammetry (DPV) were used to characterize the imprinted sensor. The results indicated that the imprinted electrode based on Gr/CNTs 3D nanocomposites was prepared successfully. Compared with other methods for determination of TBBPA, the imprinted sensor showed excellent selectivity and sensitivity toward TBBPA. The proposed imprinted sensor was applied to detect TBBPA in fish sample successfully.

2. Experimental

2.1. Reagents and chemicals

Graphite powder, $KMnO_4$, H_2SO_4, Bu_4NBF_4, HCl, acetonitrile, HBF_4 (50 wt% in water), *N,N′*-dicyclohexylcarbodiimide (DCC), *N*-hydroxysuccinimide (NHS), tetrahydrofuran (THF), dimethylformamide (DMF), hydrazine monohydrate, potassium ferricyanide, phenol, and H_2O_2 were obtained from Beijing Chemical Reagents Company. Bisphenol A (BPA), TBBPA, phenol, and tetrabromobisphenol S (TBBPS) were obtained from Alfa Aesar Company (Tianjin, China). Sodium nitrite ($NaNO_2$) and 4-nitroaniline were obtained from Dalian Xindi Chitin (Dalian, China). A series of phosphate buffered saline (PBS) with different pH values were prepared by KH_2PO_4 and Na_2HPO_4. All reagents were analytical reagent grade. All the solutions were prepared with ultrapure water.

2.2. Instruments and measurements

All electrochemical experiments were carried out on a CHI660B electrochemical workstation (Shanghai Chenhua Instrument Co. Ltd., China). The three-electrode system was employed with a saturated calomel electrode (SCE) as the reference electrode, a platinum wire electrode as the auxiliary electrode and modified carbon electrode as the working electrode. The carbon electrode was home-made with an efficient working size of $8\times4\ mm^2$ and the detail preparation procedure was as follows. First, acrylic-modified epoxy adhesive was wrapped up the high purity rectangular carbon electrode brush which was connected with a wire. Then the wire part was inserted through a glass tube, and the high purity rectangular carbon electrode brush was anchored onto the glass tube to form an impermeable device. The electrochemical performances of the modified electrodes were characterized with different techniques including CV and DPV. CV was carried out from –0.3 to +0.8 V with a scanning rate of 50 mV s^{-1} in 5.0 mmol L^{-1} $[Fe(CN)_6]^{3-/4-}$ PBS (pH 7.5). DPV was performed from −0.3 to +0.8 V in PBS (pH=7.5) containing different TBBPA concentrations. The morphology of the modified CE surface was obtained with a field-emission scanning electron microscope (JEOL JSM-6700F). All experiments were performed at ambient temperature.

2.3. Preparation of graphene/carbon nanotubes 3D nanocomposites

Graphene oxide (GO) was prepared from graphite powder using the Hummers method [29]. The detailed procedures of amino group terminated GO (GO-NH_2) were as follows: Firstly, 300 mg of GO was added into 200 mL of anhydrous DMF in a round-bottomed flask, and then sonicated for 2 h to form a homogeneous suspension. After that, 2.3 g of NHS and 4.16 g of DCC were added into the suspension and the mixture was stirred in water bath at 50 °C for 1 h. Then, 35 mL of ethylenediamine was added dropwise to the mixture and stirred with reflux for another 4 h. Finally, the suspension was filtered and washed with ethanol and water several times to eliminate the residues and dried under vacuum at 50 °C.

Carboxyl-functionalized CNTs (CNTs-COOH) were prepared by sonication CNTs in a concentrated nitric/sulfuric acid (1:3, v/v) mixture solution at 50 °C for 6 h. Graphene/carbon nanotubes (Gr/CNTs) 3D nanocomposites were prepared as follows: First, acryl chloride-functionalized CNTs (CNTs-COCl) were prepared by suspending 100 mg of CNTs-COOH into 20 mL of thionyl chloride and stirring for 24 h at 70 °C. Then the solid was separated, washed with anhydrous THF and dried to obtain anhydrous CNTs-COCl. After that, 20 mg of CNTs-COCl and 10 mg of GO-NH_2 were added into 20 mL of anhydrous DMF solution. The mixture was stirred at 120 °C under nitrogen atmosphere for 96 h, and the mixture was reduced using 20 mL of hydrazine monohydrate (50%, wt%) at 90 °C for 24 h. Then, the dispersion was filtrated through a nylon membrane (0.22 μm) and washed several times with ultrapure water. Finally, the Gr/CNTs 3D nanocomposites were dried in a vacuum oven at 40 °C overnight.

2.4. Fabrication of Gr/CNTs 3D nanocomposites modified MIP electrode

The detailed preparation procedures of the imprinted sensor were illustrated in Fig. 1. Firstly, bare carbon electrode was polished to a mirror-like surface with 1.0 and 0.3 μm alumina slurry and washed thoroughly with ultrapure water. Afterwards, 10 mg of Gr/CNTs 3D nanocomposites was dispersed in 2 mL of 0.5 wt% of DMF solution. Typically, 10 μL of the Gr/CNTs 3D nanocomposites suspension was dropped on the surface of the cleaned bare carbon electrode with a microinjector and dried under an infrared lamp for 30 min. By the same method, Gr/CE or CNTs/CE was prepared by dropping 10 μL of Gr or CNTs-COOH suspension on the carbon electrode surface.

Imprinted electrode was constructed by coelectrodeposition of pyrrole and the template molecule TBBPA on the surface of Gr/CNTs 3D nanocomposites modified carbon electrode using a CV scanning technique. The CV scanning was performed at the potential range of 0–0.8 V for 20 cycles at 50 mV s^{-1} in 20 mL of 0.2 mol L^{-1} pyrrol PBS (pH=7.5) containing 5.0 mg mL^{-1} TBBPA. After electropolymerization, the MIP modified carbon electrode based on Gr/CNTs 3D nanocomposites (MIP/Gr/CNTs/CE) was immersed in methanol/acetic acid (9:1, v/v) mixture solution to remove the template TBBPA until TBBPA could not be detected in the elution with ultraviolet spectrograph at 209 nm.

For comparison, non-imprinted polymers (NIP) modified electrode based on Gr/CNTs 3D nanocomposites (NIP/Gr/CNTs/CE) was prepared by the same procedures without addition of the template TBBPA in the electrodeposition process.

2.5. Sample preparation

After homogenizing the fish with an Ultra-Turrax mixer, a 10.0 g aliquot was transferred into a 50 mL centrifuge tube. Then 10 mL of acetonitrile and 10 mL of hexane were added and the mixture was shaken for 90 s. After centrifugation at a speed of 3000 rpm for 20 min, the solution was transferred into a beaker. The solid residue and the hexane phase were extracted for a second time by adding a fresh 10 mL of acetonitrile. The acetonitrile extracts were filtered with 0.45 μm membrane and the filtrate was evaporated under a constant stream of nitrogen for

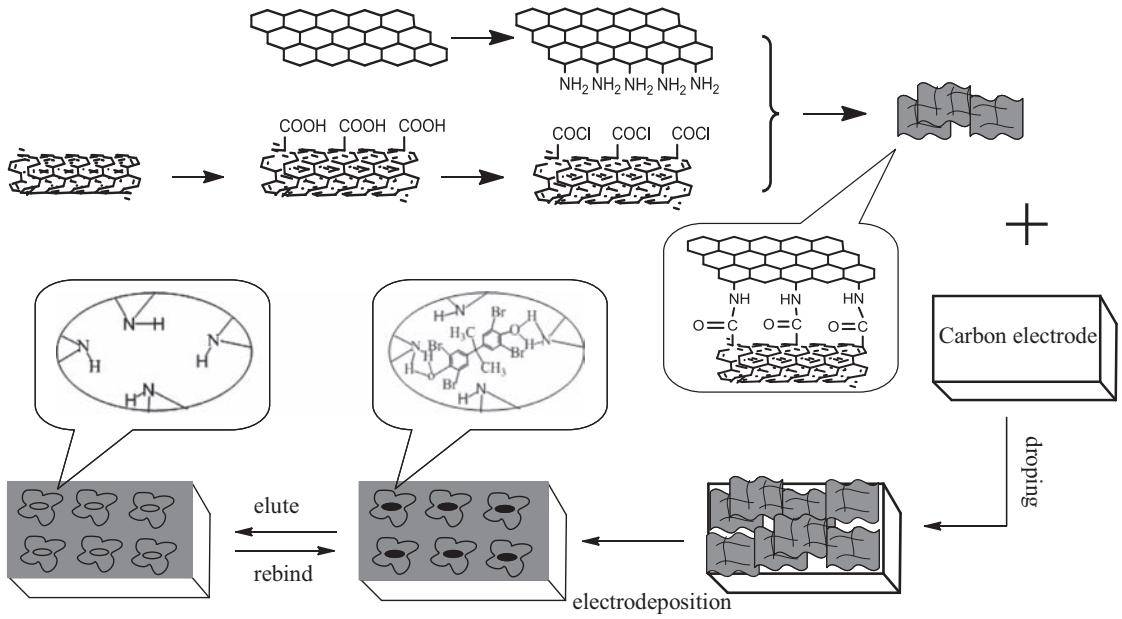

Fig. 1. Preparation procedure of TBBPA imprinted electrochemical sensor.

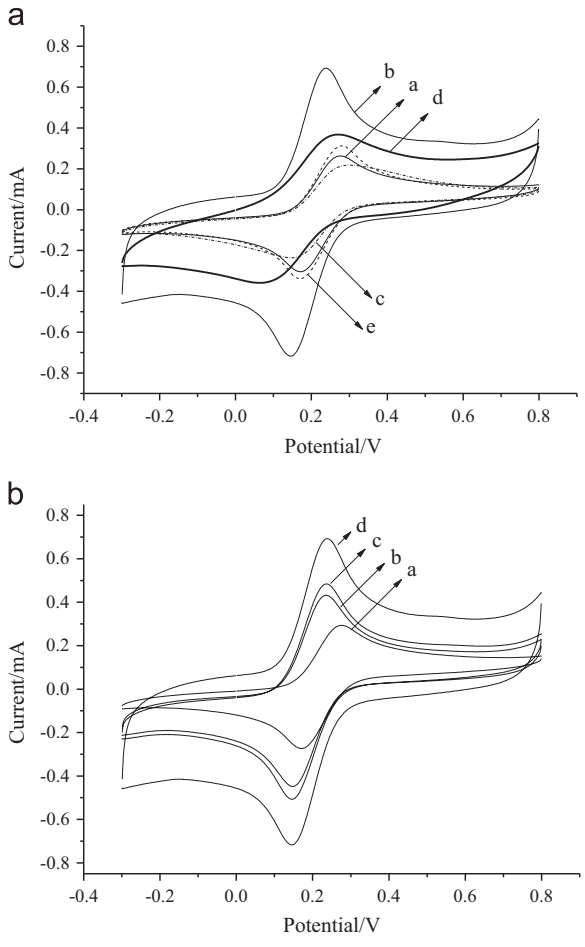

Fig. 2. (A) CV of the bare CE (a), Gr/CNTs/CE (b), MIP/Gr/CNTs/CE containing the template (c), MIP/Gr/CNTs/CE without the template (d) and NIP/Gr/CNTs/CE (e); (B) CV of the bare CE (a), CNTs/CE (b), Gr /CE (c) and Gr/CNTs/CE (d) in 5.0 mmol L^{-1} $[Fe(CN)_6]^{3-/4-}$ PBS (pH 7.5). Scanning rate is 50 mV s^{-1}.

2.0 mL. After diluting the mixture to the ratio 1:10 with PBS solution (pH=7.5), it was stored in a refrigerator under 4 °C before use.

3. Results and discussion

3.1. Preparation and characterization of MIP/Gr/CNTs/CE

Prior to 3D nanocomposites modified on the electrode surface, the chemical structures of CNTs-COOH, GO-NH_2 and Gr/CNTs nanocomposites have been investigated by Fourier-transform infrared (FT-IR) spectrum analysis. As shown in Fig. S1, the FT-IR spectrum of GO-NH_2 shows an absorption band at 3327 cm^{-1}, which is characteristic of the –OH group. The adsorption bands at 1580 cm^{-1} and 641 cm^{-1} correspond to the –NH- and –CO–NH- bending vibration, respectively. And the band at 1088 cm^{-1} corresponds to the C–N stretching vibration. The FT-IR spectrum of CNTs-COOH shows an absorption band at 3329 cm^{-1}, which was assigned to –OH stretching vibration. After combined CNTs-COOH and GO-NH_2 to form Gr/CNTs, bending vibration of the –CO–NH- at 3370 cm^{-1}, C–N stretching vibration at 1088 cm^{-1} and –NH-bending vibration at 640 cm^{-1} appeared. These results indicated that the Gr/CNTs nanocomposites were fabricated successfully.

In this paper, $[Fe(CN)_6]^{3-/4-}$ was chosen as an indicator to investigate the electrodes' electrochemical behavior. The electrochemical behavior of stepwise fabrication process of the electrode was studied in 5.0 mmol L^{-1} $[Fe(CN)_6]^{3-/4-}$ PBS (pH=7.5). As shown in Fig. 2A, a couple of redox peaks were existed for the bare CE. When the electrode surface was covered with the Gr/CNTs 3D nanocomposites, the redox peak currents increased apparently, indicating the modified Gr/CNTs 3D nanocomposites can improve the sensitivity of the Gr/CNTs/CE. In Fig. 2B, redox peaks of the Gr/CNTs/CE were larger than that of sole Gr or CNTs modified CE. The increment of peak currents can be attributed to the synergistic effect of the Gr and CNTs, which can improve the electrical conductivity and activation area of the Gr/CNTs 3D nanocomposites modified electrode [30]. Curve c in Fig. 2A shows the cyclic voltammogram of MIP/Gr/CNTs/CE before removing the template. Compared with CV of the Gr/CNTs/CE, the peak currents of the MIP/Gr/CNTs/CE before removing the template reduced due to the modification of MIP film on the electrode surface. After TBBPA removal, an obvious increment of the peak currents was obtained compared to the peak currents of the MIP/Gr/CNTs/CE before removing the template, which was caused by the formation of

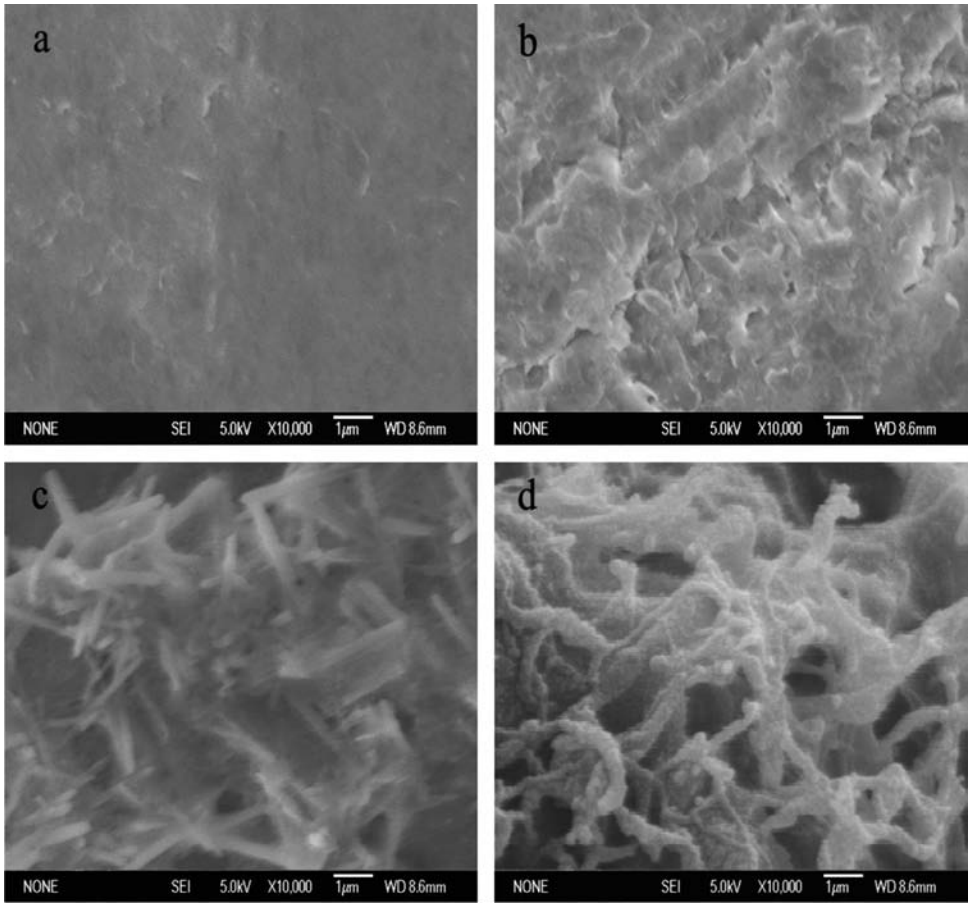

Fig. 3. SEM images of the bare electrode (a), Gr/CE (b), Gr/CNTs/CE (c) and MIP/Gr/CNTs/CE (d).

vacant binding cavities which can accelerate mass transfer and electronic transmission. Curve e in Fig. 2A is the cyclic voltammogram of the NIP/Gr/CNTs/CE, which was apparently lower than that of the MIP/Gr/CNTs/CE after removing the template. The reason was that there was no imprinted cavity on the surface of the NIP/Gr/CNTs/CE for the probe $[Fe(CN)_6]^{3-/4-}$ to pass through.

The SEM images of the surface of bare CE, Gr/CE, Gr/CNTs/CE and MIP/Gr/CNTs/CE were shown in Fig. 3. The SEM image of the bare carbon electrode shows a smooth morphology. The Gr modified electrode displays a typical crumpled and wrinkled surface. When the Gr/CNTs were grafted, a three-dimensional network structure was observed onto the surface of the CE, which improved the Gr/CNTs/CE specific area. After electropolymerization of the MIP film, the surface of the MIP/Gr/CNTs/CE became rougher than that of the Gr/CNTs/CE, indicating that the MIP film has been uniformly deposited onto the Gr/CNTs/CE.

3.2. Effect of pH

The influence of $[Fe(CN)_6]^{3-/4-}$ solution with different pHs range of 5.8–8.5 on the electrochemical performance of the MIP/Gr/CNTs/CE toward TBBPA (1.0×10^{-10} mol L^{-1}) was studied with DPV technique in this paper. $[Fe(CN)_6]^{3-/4-}$ was chosen as an indicator based on TBBPA could not occur electrochemical reaction on the imprinted sensor unless $[Fe(CN)_6]^{3-/4-}$ probe being added [16]. As shown in Fig. 4A, a maximum response current (ΔI_p, which is equal to the blank peak value minus the real response peak current) was observed at pH 7.5, indicating that when the solution pH is 7.5, the interaction between TBBPA and the imprinted film can be facilitated. It is a fact that TBBPA has two proton-binding sites, carboxyl and piperazinyl group with pK_a values of 7.5 and 8.5, respectively [31]. When the solution pH is less than 7.5, the hydroxyl competitively adsorbed onto the imprinted sites in the MIP/Gr/CNTs/CE with anionic TBBPA decreased the uptake of TBBPA. At pH > 7.5, the TBBPA was mainly in the form of negatively charged phenoxy ion, while the electrostatic repulsion between the imprinted sites in the MIP/Gr/CNTs/CE and phenoxy anions lead to a decrease of imprinting bind [32]. Meanwhile, the response currents of the MIP/Gr/CNTs/CE were higher than that of the NIP/Gr/CNTs/CE, which suggested that binding sites were existed in the imprinted film.

3.3. Optimization of scanning cycles

Studies showed the thickness of polymer film could be adjusted easily by controlling the number of scanning cycles during the electropolymerization process [33]. The optimized cyclic scanning cycles of electropolymerization for preparation of an excellent imprinted sensor was investigated by comparing the response currents of the different MIP/Gr/CNTs/CEs prepared by different CV scanning cycles toward 1.0×10^{-10} mol L^{-1} TBBPA. As shown in Fig. 4B, the response current of the MIP/Gr/CNTs/CE prepared with CV scanning for 20 cycles reached the maximum in 5.0 mmol L^{-1} $[Fe(CN)_6]^{3-/4-}$ PBS (pH = 7.5) containing 1.0×10^{-10} mol L^{-1} TBBPA, and then decreased with the further increment of scanning cycles. In general, when the imprinted film was too thick, the template molecules were situated at the central area of the imprinted film, which resulted in the template molecules removed from the imprinted film incompletely. Thus, 20 cycles was selected as an optimal scanning cycles to provide the highest sensitivity of the imprinted film toward TBBPA.

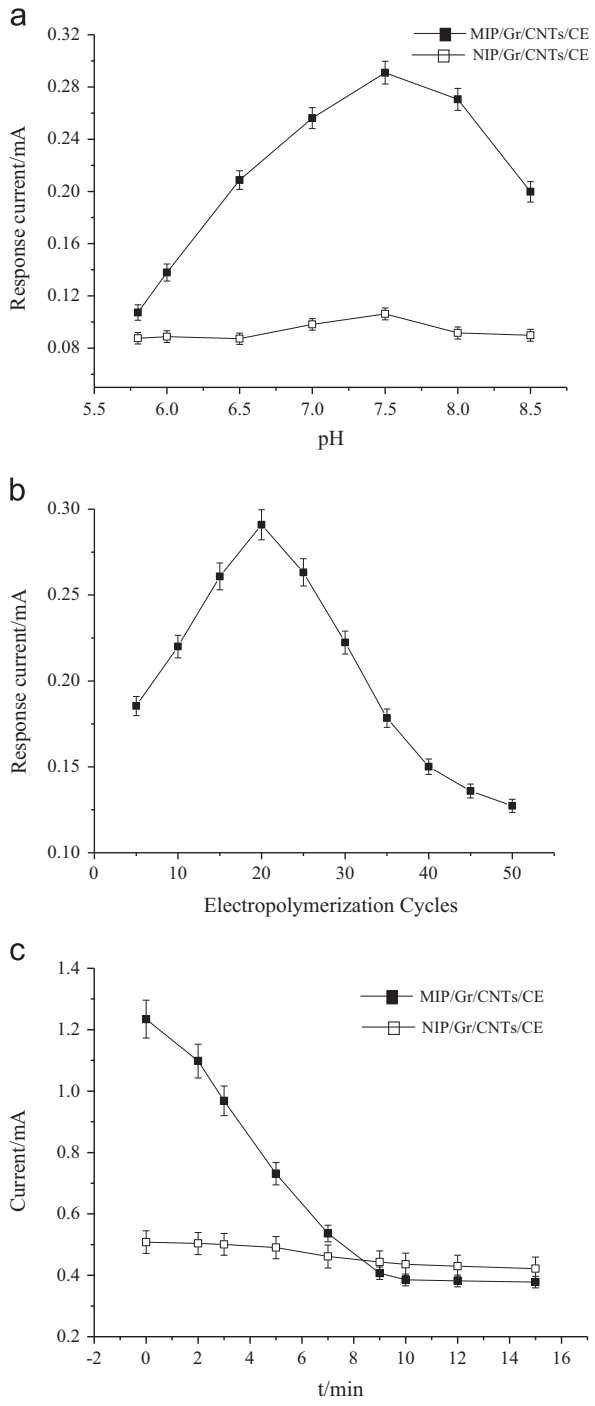

Fig. 4. (A) Effect of different pH values on the response of the MIP/Gr/CNTs/CE; (B) effect of the different scanning cycles on the response of the MIP/Gr/CNTs/CE in 5.0 mmol L^{-1} $[Fe(CN)_6]^{3-/4-}$ PBS (pH 7.5); (C) curve of adsorption kinetics of the MIP/Gr/CNTs/CE and NIP/Gr/CNTs/CE toward TBBPA. The concentration of TBBPA was 1.0×10^{-10} mol L^{-1}.

3.4. Adsorption kinetics of MIP/Gr/CNTs/CE

The binding kinetic of the MIP/Gr/CNTs/CE toward TBBPA was investigated by changing the adsorption interval time range of 2–15 min in 1.0×10^{-10} mol L^{-1} of TBBPA solution. As shown in Fig. 4C, the rebinding amount of TBBPA on the MIP/Gr/CNTs/CE increased quickly in the interval time of 0–10 min, resulting in the rapid decrement of the response currents. After that, the response currents remained almost constant when the MIP/Gr/CNTs/CE was immersed in TBBPA solution over 10 min. However, little of current changes were observed with the increment of the time when the NIP/Gr/CNTs/CE was immersed in TBBPA solution. This could be explained that most imprinted cavities were situated at the surface of the MIP film, which resulted in the recognition sites fast combination with the template molecule and a shorter time was needed for the MIP/Gr/CNTs/CE to reach binding equilibrium.

3.5. Calibration curve

DPV was conducted to detect TBBPA standard solutions with different concentrations range of 1.0×10^{-11}–1.0×10^{-8} mol L^{-1} to investigate the analytical performance of the MIP/Gr/CNTs/CE. As depicted in Fig. 5A, the peak currents decreased with the increment of the concentration of TBBPA, the response mechanism can be explained that the TBBPA molecules diffuse to the electrode combining with the imprinted cavities, in which $[Fe(CN)_6]^{3-/4-}$ acting as probe cross through the imprinted film to reach the carbon electrode. Thus the more the TBBPA combined, the more the current responded. Furthermore, the response current (ΔI_p) of the MIP/Gr/CNTs/CE was linear toward the negative logarithm of TBBPA concentration ($-\log C$) ranged from 1.0×10^{-11} to 1.0×10^{-8} mol L^{-1}. As shown in Fig. 5B, the linear equation is as follows:

$$\Delta I_p = 1.356 + 0.105 \log C \left(R^2 = 0.991\right)$$

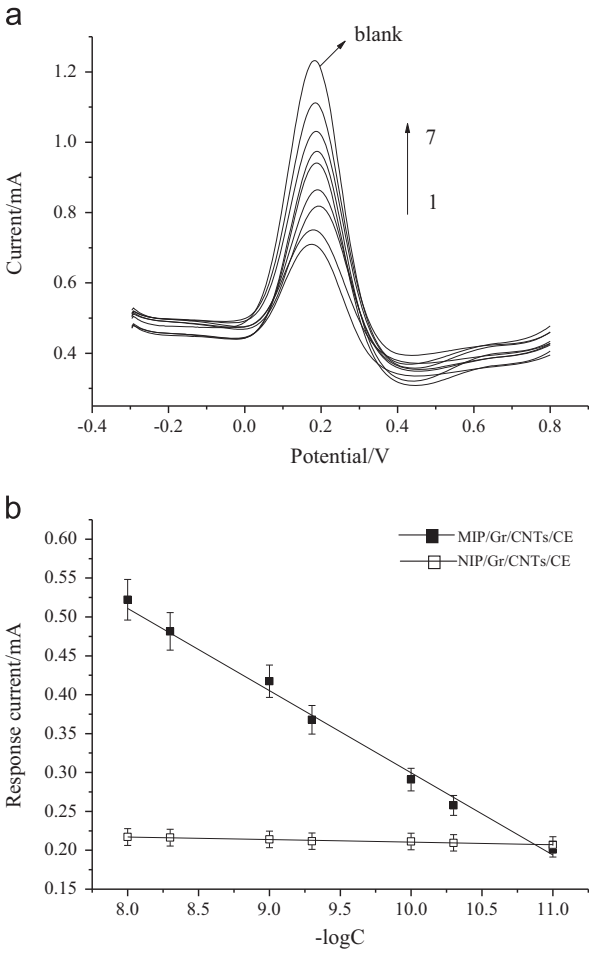

Fig. 5. (A) DPV responses of the MIP/Gr/CNTs/CE toward different TBBPA concentrations (1, 2, 3, 4, 5, 6 and 7 correspond to TBBPA concentration of 1.0×10^{-8}, 5.0×10^{-9}, 1.0×10^{-9}, 5.0×10^{-10}, 1.0×10^{-10}, 5.0×10^{-11} and 1.0×10^{-11} mol L^{-1}, respectively); (B) calibration curve of the MIP/Gr/CNTs/CE response currents toward different TBBPA concentrations. The blank peak value is 1.23 mA.

Table 1
Comparison with other reported methods for determination of TBBPA.

Analytical methods[a]	Detection limit	Recovery (%)	Applications	References
MIP-SPE–LC/DAD	2 ng L^{-1}	85–97	Tap water, river water and lake water	34
MIP-SPE–HPLC	2.2–3.8 ng L^{-1}	89.4–102.0	Tap water and river water	35
MIP-SPE–HPLC	3 ng L^{-1}	95–105	Tap water	36
SPE–HPLC	0.4–0.9 μg L^{-1}	86.5–103.6	River water and waste water	37
MIP–luminescent sensor	1.5×10^{-8} mol L^{-1}	80.2–96.5	Water and soil	12
MIP–electrochemical sensor	2.3×10^{-10} mol L^{-1}	101–104	Rain and lake water	16
MIP–electrochemical sensor	1.3×10^{-10} mol L^{-1}	100.1–104	Tap water, rain and lake water	17
MIP–electrochemical sensor	3.7×10^{-12} mol L^{-1}	93.3–107.7	Catfish, Chub, Carp sample	In this paper

[a] MIP-SPE: molecularly imprinted polymer-solid phase extraction; LC/DAD: liquid chromatography combined with diode array detector; HPLC: high performance liquid chromatography.

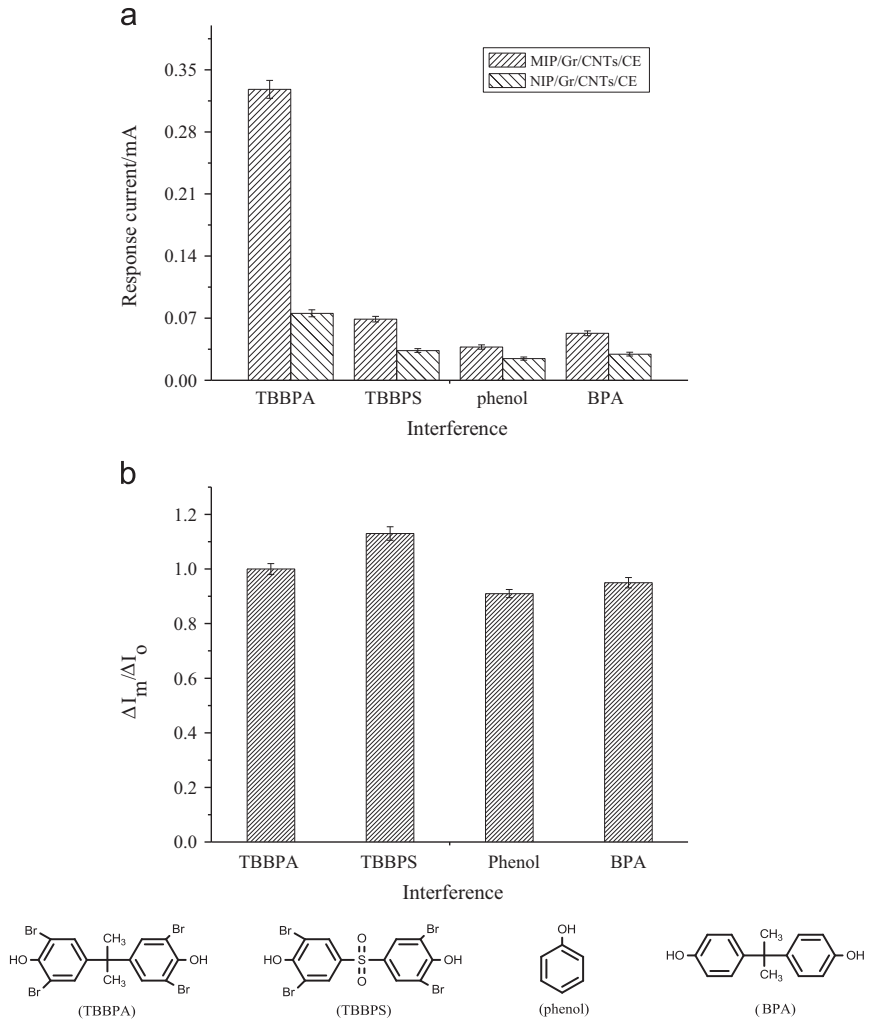

Fig. 6. (A) DPV responses of MIP/Gr/CNTs/CE and NIP/Gr/CNTs/CE toward 1.0×10^{-10} mol L^{-1} TBBPA and structural analogs; (B) peak current ratio ($\Delta I_m/\Delta I_o$) of MIP/Gr/CNTs/CE to 1.0×10^{-10} mol L^{-1} TBBPA and 1.0×10^{-10} mol L^{-1} TBBPA in the presence of 5.0×10^{-9} mol L^{-1} TBBPS, phenol and BPA, respectively. And the bottom of the figure is chemical structure of TBBPS, phenol and BPA.

The detection limit was calculated as 3.7×10^{-12} mol L^{-1} at a signal-to-noise ratio of 3, which was more sensitive than most available TBBPA detection methods shown in Table 1 [16,17,34–37].

3.6. Selectivity

To study the selectivity of the proposed MIP/Gr/CNTs/CE sensor, DPV response currents of the MIP/Gr/CNTs/CE and NIP/Gr/CNTs/CE toward TBBPA and structural analogs were investigated and the results were shown in Fig. 6A. The response currents at 0.2 V of the MIP/Gr/CNTs/CE toward TBBPA were larger than that of the NIP/Gr/CNTs/CE. And the ΔI_p of the MIP/Gr/CNTs/CE toward TBBPA was larger than that toward structural analogs either, which revealed that the proposed MIP/Gr/CNTs/CE exhibited good selectivity towards TBBPA. The high selectivity of the MIP/Gr/CNTs/CE toward TBBPA was ascribed to the molecular interaction between TBBPA and the amino groups of the functional monomers in the specific recognition sites of the imprinted polymers. Only the template molecule TBBPA can enter and combine with the imprinted cavities due to the compatibility of molecule size between the

Table 2
Determination of TBBPA in fish samples ($n=3$).

Sample	Sample content[a] ($\times 10^{-9}$ mol L^{-1})	Added ($\times 10^{-9}$ mol L^{-1})	Found ($\times 10^{-9}$ mol L^{-1})	Recovery (%)	RSD (%)
Catfish	6.3 ± 0.2	1.0	7.5 ± 0.1	102.7	3.6
		2.0	8.2 ± 0.2	98.8	4.3
		3.0	9.4 ± 0.1	101.1	3.7
Chub	–	1.0	1.1 ± 0.1	110.0	3.5
		2.0	1.9 ± 0.1	95.0	3.9
		3.0	2.8 ± 0.2	93.3	4.0
Carp	0.9 ± 0.1	1.0	1.8 ± 0.1	94.7	4.1
		2.0	3.1 ± 0.2	106.9	3.3
		3.0	4.2 ± 0.2	107.7	3.9

[a] TBBPA in sample content was detected with HPLC.

imprinted cavity and TBBPA. Furthermore, the selectivity of the MIP/Gr/CNTs/CE towards TBBPA was valued by the response current ratio ($\Delta I_m/\Delta I_o$, ΔI_m and ΔI_o are response current of TBBPA at 0.2 V in the presence and absence of interferences.) of DPV response in the presence of structural analogs including TBBPS, phenol and BPA. As shown in Fig. 6B, comparison with reference response current ratio of TBBPA ($\Delta I_m/\Delta I_o=1$), $\Delta I_m/\Delta I_o$ was only slightly changed from 91.0% to 113.0% with 50-fold of interfering substances.

3.7. Reproducibility, repeatability and stability

The reproducibility of the MIP/Gr/CNTs/CE was investigated for 1.0×10^{-10} mol L^{-1} TBBPA. The response currents of five MIP/Gr/CNTs/CEs which were prepared with the same procedure toward the TBBPA were investigated. A relative standard deviation of 3.1% for the five MIP/Gr/CNTs/CEs confirmed that the imprinted sensor modified with Gr/CNTs 3D nanocomposites in this paper is reproducible. The MIP/Gr/CNTs/CE could be used at least 50 or 60 times with subsequent washing and measuring operations with the relative standard deviation (RSD) of 3.5%. Moreover, no apparent decrease in the response currents of the MIP/Gr/CNTs/CE toward 1.0×10^{-10} mol L^{-1} was found when it was stored for 1 month.

3.8. Applications

To ascertain the feasibility of the novel MIP/Gr/CNTs/CE for its possible application, the MIP/Gr/CNTs/CE was used for testing three fish samples and evaluating the recovery of TBBPA. Each sample was tested for three times. As shown in Table 2, TBBPA was only found in the Catfish sample and Carp sample, and the recoveries were in the range of 93.3–107.7%, indicating that the MIP/Gr/CNTs/CE can be applied for the determination of TBBPA in the real sample.

4. Conclusions

A sensitive and selective imprinted sensor based on Gr/CNTs 3D nanocomposites was constructed successfully for the determination of TBBPA in this paper. The excellent performance of the MIP/Gr/CNTs/CE for the determination of TBBPA was ascribed to the synergistic effects of the good electrical conductivity of Gr/CNTs 3D nanocomposites and the selectivity of the imprinted film. With excellent sensitivity and selectivity, the MIP/Gr/CNTs/CE was applied to analysis of real samples successfully with the recoveries of 93.3–107.7%. This work provides a general protocol to fabricate 3D hybrid nanocomposites modified sensor for sensitive and selective persistent environmental pollutants detection.

Acknowledgments

This work is supported by the National Natural Science Foundation of China (No. 21267010), the Open Foundation of Institute of Environmental Chemistry and Ecotoxicology State Key Laboratory (No. KF2011-25).

Appendix A. Supporting information

Supplementary data associated with this article can be found in the online version at http://dx.doi.org/10.1016/j.talanta.2014.11.040.

References

[1] A. Covaci, S. Harrad, M.A.E. Abdallah, N. Ali, R.J. Law, D. Herzke, C.A. de Wit, Environ. Int. 37 (2011) 532–556.
[2] H. Huang, S. Zhang, P. Christie, S. Wang, M. Xie, Environ. Sci. Technol. 44 (2010) 663–667.
[3] M. Alaee, P. Ariasb, A. Sjödinc, A. Bergmand, Environ. Int. 29 (2003) 683–689.
[4] M.A.E. Abdallah, S. Harrad, A. Covaci, Environ. Sci. Technol. 42 (2008) 6855–6861.
[5] A. Covaci, S. Voorspoels, M.A.E. Abdallah, T. Geens, S. Harrad, R.J. Law, J. Chromatogr. A 1216 (2009) 346–363.
[6] M.J. He, X.J. Luo, L.H. Yu, J. Liu, X.J. Zhang, S.J. Chen, D. Chen, B.X. Mai, Environ. Sci. Technol. 44 (2010) 5748–5754.
[7] J.P. Wu, Y. Zhang, X.J. Luo, Y.Z. She, L.H. Yu, S.J. Chen, B.X. Mai, J. Environ. Sci. 24 (2012) 183–194.
[8] M. Samuelsen, C. Olsen, J.A. Holme, E. Meussen-Elholm, A. Bergmann, J.K. Hongslo, Cell Biol. Toxicol. 17 (2001) 139–151.
[9] G. ten Dama, O. Pardo, W. Traag, M. van der Lee, R. Peters, J. Chromatogr. B: Anal. Technol. Biomed. Life Sci. 898 (2012) 101–110.
[10] R.S. Zhao, S.S. Wang, C.G. Cheng, L.L. Zhang, X. Wang, Chromatographia 73 (2011) 793–797.
[11] L.C. Dirtu, L. Roosens, T. Geens, A. Gheorghe, H. Neels, A. Covaci, Anal. Bioanal. Chem. 391 (2008) 1175–1181.
[12] Y.P. Chen, D.N. Wang, Y.M. Yin, L.Y. Wang, X.F. Wang, M.X. Xie, J. Agric. Food Chem. 60 (2012) 10472–10479.
[13] X. Kang, J. Wang, H. Wu, J. Liu, I.A. Aksay, Y. Lin, Talanta 81 (2010) 754–759.
[14] Y. Li, X. Li, C.K. Dong, J.Y. Qi, X.J. Han, Carbon 48 (2010) 3427–3433.
[15] Y.Q. Wang, Y.Y. Yang, L. Xu, J. Zhang, Electrochim. Acta 56 (2011) 2105–2109.
[16] H.J. Chen, Z.H. Zhang, R. Cai, X.Q. Kong, X. Chen, Y.N. Liu, S.Z. Yao, Analyst 138 (2013) 2769–2776.
[17] H.J. Chen, Z.H. Zhang, R. Cai, W. Rao, F. Long, Electrochim. Acta 117 (2014) 385–392.
[18] J. Yan, T. Wei, B. Shao, F.Q. Ma, Z.J. Fan, M.L. Zhang, C. Zheng, Y.C. Shang, W.Z. Qian, F. Wei, Carbon 48 (2010) 1731–1737.
[19] S.Q. Chen, P. Chen, Y. Wang, Nanoscale 3 (2011) 4323–4329.
[20] Z.J. Fan, J. Yan, L.J. Zhi, Q. Zhang, T. Wei, J. Feng, M.L. Zhang, W.Z. Qian, F. Wei, Adv. Mater. 22 (2010) 3723–3728.
[21] Q. Cheng, J. Tang, J. Ma, H. Zhang, N. Shinya, L.C. Qin, Phys. Chem. Chem. Phys. 13 (2011) 17615–17624.
[22] V.C. Tung, L.M. Chen, M.J. Allen, J.K. Wassei, K. Nelson, R.B. Kaner, Y. Yang, Nano Lett. 9 (2009) 1949–1955.
[23] E. Yoo, J. Kim, E. Hosono, H. Zhou, T. Kudo, I. Honma, Nano Lett. 8 (2008) 2277–2282.
[24] X.J. Lu, H. Dou, B. Gao, C.Z. Yuan, S.D. Yang, L. Hao, L.F. Shen, X.G. Zhang, Electrochim. Acta 56 (2011) 5115–5121.
[25] E. Turiel, A. Martín-Esteban, Anal. Chim. Acta 668 (2010) 87–99.
[26] S. Suriyanarayanan, P.J. Cywinski, A.J. Moro, G.J. Mohr, W. Kutner, Top. Curr. Chem. 325 (2012) 165–265.

[27] H.J. Chen, Z.H. Zhang, L.J. Luo, S.Z. Yao, Sens. Actuat. B—Chem. 163 (2012) 76–83.
[28] M. Javanbakht, F. Fathollahi, F. Divsarb, M.R. Ganjalic, P. Norouzic, Sens. Actuat. B—Chem. 182 (2013) 362–367.
[29] W.S. Hummers, R.E. Offeman, J. Am. Chem. Soc. 80 (1958) (1339–1339).
[30] X.C. Dong, B. Li, A. Wei, X.H. Cao, M.B. Chan-Park, H. Zhang, L.J. Li, W. Huang, P. Chen, Carbon 49 (2011) 2944–2949.
[31] Y. Zhang, Y. Tang, S. Li, S. Yu, Chem. Eng. J. 222 (2013) 94–100.
[32] I.I. Fasfous, E.S. Radwan, J.N. Dawoud, Appl. Surf. Sci. 256 (2010) 7246–7252.
[33] D.M. Gao, Z.P. Zhang, M.L. Wu, C.G. Xie, G.J. Guan, D.P. Wang, J. Am. Chem. Soc. 129 (2007) 7859–7866.
[34] Y.M. Yin, Y.P. Chen, X.F. Wang, Y. Liu, H.L. Liu, M.X. Xie, J. Chromatogr. A 1220 (2012) 7–13.
[35] X.L. Sun, J.C. Wang, Y. Li, J. Jin, B.Q. Zhang, S.M. Shah, X.L. Wang, J.P. Chen, J. Chromatogr. A 1343 (2014) 33–41.
[36] J. Li, X.B. Zhang, Y.X. Liu, H.W. Tong, Y.P. Xu, S.M. Liu, Talanta 117 (2013) 281–287.
[37] X.M. Wang, J.Y. Liu, A.F. Liu, Q. Liu, X.Z. Du, G.B. Jiang, Anal. Chim. Acta 753 (2012) 1–7.